

---

# Image2Point: 3D Point-Cloud Understanding with Pretrained 2D ConvNets

---

Chenfeng Xu<sup>1</sup>   Shijia Yang<sup>1</sup>   Bohan Zhai<sup>1</sup>   Bichen Wu<sup>2\*</sup>   Xiangyu Yue<sup>1</sup>

Wei Zhan<sup>1</sup>

Peter Vajda<sup>2</sup>

Kurt Keutzer<sup>1</sup>

Masayoshi Tomizuka<sup>1</sup>

<sup>1</sup> University of California, Berkeley

<sup>2</sup> Facebook Inc

{xuchenfeng, shijiayang, zhaibohan, xyyue, wzhan, keutzer}@berkeley.edu,  
{wbc, vajdap}@fb.com,  
tomizuka@me.berkeley.edu

## Abstract

3D point-clouds and 2D images are different visual representations of the physical world. While human vision can understand both representations, computer vision models designed for 2D image and 3D point-cloud understanding are quite different. Our paper investigates the potential for transferability between these two representations by empirically investigating whether this approach works, what factors affect the transfer performance, and how to make it work even better. We discovered that we can indeed use the same neural net model architectures to understand both images and point-clouds. Moreover, we can transfer pretrained weights from image models to point-cloud models with minimal effort. Specifically, based on a 2D ConvNet pretrained on an image dataset, we can transfer the image model to a point-cloud model by *inflating* 2D convolutional filters to 3D then finetuning its input, output, and optionally normalization layers. The transferred model can achieve competitive performance on 3D point-cloud classification, indoor and driving scene segmentation, even beating a wide range of point-cloud models that adopt task-specific architectures and use a variety of tricks. The code is available at: <https://github.com/chenfengxu714/image2point>.

## 1 Introduction

A point-cloud is an important visual representation for 3D computer vision. It is widely used in applications such as autonomous driving [1, 2, 3], robotics [4, 5, 6], augmented and virtual reality [7, 8, 9], *etc.* A point-cloud represents visual information in a highly different way from a 2D image. A point-cloud essentially consists of a set of unordered points, with each point encoding its spatial x, y, z coordinates and potentially other features. In contrast, a 2D image organizes visual features as a dense 2D pixel array. Due to the representation differences, 2D image and 3D point-cloud understanding are treated as separate problems. Image models and point-cloud models are designed to have different architectures and are trained on different types of data. Few research efforts have tried to directly transfer models from images to point-clouds or vice versa.

---

\*Corresponding Author

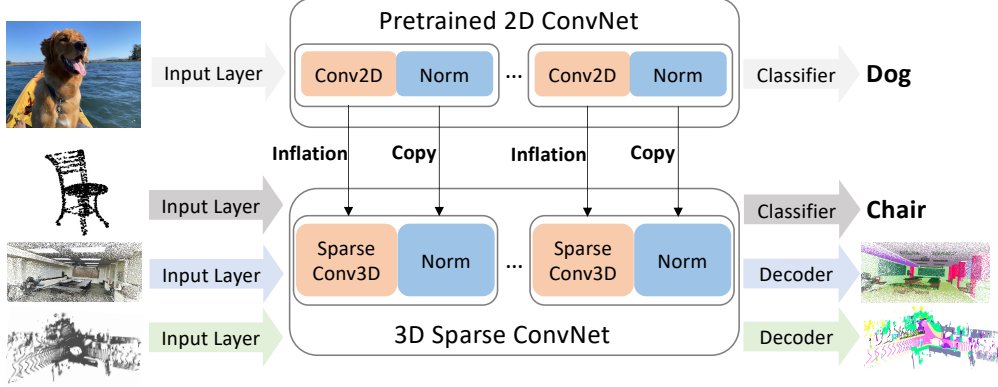


Figure 1: We investigate the feasibility of pretrained 2D ConvNets transferring to 3D sparse ConvNets. With filter inflation and finetuning only the input, output layer (classifier for classification task and decoder for semantic segmentation task), and optionally normalization layers, 3D Sparse ConvNets are capable of dealing with point-cloud classification, indoor, and driving scene segmentation.

Intuitively, both 3D point-clouds and 2D images are visual representations of the physical world. Their low-level representations are drastically different, but they can represent the same underlying visual concept. Furthermore, human vision has no problem understanding both representations. Therefore, we explore whether computer vision models trained on one modality can be used to understand the other.

Somewhat surprisingly, the answer to the question immediately above is: yes, 2D image models trained on image datasets can be transferred to understand 3D point-clouds with minimal effort. As illustrated in Figure 1, we transfer a 2D ConvNet to a 3D ConvNet whose input is a 3D voxel representation converted from a point-cloud. Based on a pretrained 2D ConvNet, we *inflate* its 2D convolutional filters to 3D by copying the filter weights along a third dimension. We add input and output layers to the network, and on a target point-cloud dataset, we only finetune the input/output layers and optionally the normalization layers, while keeping the original model weights untouched. This transferred model can achieve competitive performance with 88.09% top 1 accuracy, 55.22% mIoU, and 58.76% mIoU for CAD model classification, indoor and outdoor semantic segmentation, respectively, outperforming many previous point-cloud models that adopt task-specific model architectures and tricks. When trained on a small number of samples, the transferred model drastically outperforms the model trained from scratch, exhibiting superior data efficiency with 11.26% accuracy improvement in extremely low data regime on the ModelNet 3D Warehouse dataset.

Transferring models from images to point-clouds has several potential benefits: 1) recent research has shown that pretrained image models effectively improve the downstream task’s performance [10]. 2) pretrained image models also drastically improve data efficiency on downstream tasks, even enabling promising few-shot or zero-shot transfer [10, 11, 12, 13]. This is particularly interesting for point-cloud understanding as obtaining and annotating point-clouds are difficult and expensive [14].

In order to better understand whether we can transfer the image model to point-cloud, whether we can utilize benefits of the recent progress of image representation learning, what factors impact the performance, and how we can make it work better, we design eight questions and provide experimental results to these questions. Our experiments show that 1) transferring image models to point-cloud understanding is feasible; 2) we observe preliminary but promising results that pretrained image models can improve downstream task performance and data efficiency; 3) however, we also note some phenomenon that contradicts our expectations from image-to-image transfer. For example, bigger datasets do not necessarily improve or even hurt downstream performance; stronger pretrained models do not necessarily yield better downstream performance. These findings indicate future research is needed to unlock the potential of transferring image models to point-cloud understanding.

## 2 Related Work

### 2.1 Point-cloud processing model

**3D convolution-based method** is one of the mainstreams in point-cloud processing approaches which efficiently process point-clouds based on voxelization. In particular, in this approach, voxelization is used to rasterize point-cloud into regular grids (called voxels), thus conventional 3D convolutions can be applied. Sparse convolution is proposed to apply on the non-empty voxels [15, 16, 17, 18, 19], largely improving the efficiency of 3D convolutions.

**Projection-based method** attempts to project a 3D point-cloud to a 2D plane and use 2D convolution to extract features [20, 21, 22, 23, 24, 25, 26]. Specifically, the bird-eye-view projection [27, 28] and the spherical projection [21, 22, 23, 29] make great progress in outdoor point-cloud tasks.

**Point-based method** directly processes the point-cloud data. The most classic method, PointNet [30] and PointNet++ [31], directly consume by customized feature aggregation. Many works further develop advanced local-feature aggregation operators that mimic the convolution to structure data [6, 32, 33, 34, 35, 36, 37, 38, 39].

### 2.2 Pretraining in 2D and 3D vision

**Pretraining in 2D vision** has shown effectiveness under supervised [40, 41], self-supervised [42, 43], and unsupervised contrastive approach [12, 44, 11, 45, 46, 47]. After pretraining on a large amount of image data, a 2D model requires much fewer computational resources and data for later finetuning to reach competitive performance on downstream tasks [48, 49, 50, 51].

**Pretraining in 3D vision** has been studied similarly as pretraining in 2D vision: both self-supervised and contrastive pretraining [52] show promising results. Due to the lack of large, annotated point-cloud datasets, pretraining in 3D vision is motivated for data efficiency [53]. Recent works [54, 55] consider pretraining methods, for example, Contrastive Scene Contents which making use of both point-level correspondences and spatial contexts, with data efficiency in mind.

### 2.3 Cross-modal learning

**Cross-modal learning** attempts to take advantage of a data modality that is different from the data modality of the downstream task [56, 57]. For example, xMUDA [58] utilizes aligned images and point-clouds to transfer 2D feature map information for 3D semantic segmentation through knowledge distillation [59]. For cross-modal transfer learning [60], Liu et al. [61] proposed pixel-to-point knowledge transfer (PPKT) from 2D to 3D which uses aligned RGB and RGB-D images during pretraining. Our work does not rely on joint image-point-cloud pretraining. Instead, we directly transfer an image-pretrained model to point-cloud with the simplest pretraining-finetuning scheme.

Some of the previous works for video and medical images [62, 63] have discussed 2D-3D transfer learning by simply extending a 2D filter along time or depth direction to transfer pretrained 2D filters to 3D models. In this work, we study in depth for point-cloud models that, with a similar approach, we are able to reach a comparable performance with training from scratch, but only finetuning input and output layers. Between language and image modality, transfer learning with minimal finetuning also shows a competitive performance [64].

## 3 Converting a 2D ConvNet to a 3D ConvNet

In this paper, we mainly focus on the 3D sparse-convolution based method to process point-clouds. As discussed in 2.1, we consider a set of points where each point is parameterized by its 3D coordinates and optionally additional features such as intensity and RGB. We then voxelize/quantize these points into voxels according to their 3D space coordinates, following [16]. A voxel’s feature is inherited from the point that lies in the voxel. If there are multiple points in a voxel, then we average all points’ feature and assign the mean to the voxel. If there is no point in the voxel, then we simply set the voxel’s feature to 0. When using sparse convolution, we skip the computation on empty voxels.

Given a pretrained 2D ConvNet, we convert it to a 3D ConvNet that takes 3D voxels as input. The key element of this procedure is to convert 2D convolutions to 3D. A 2D convolutional filter can be

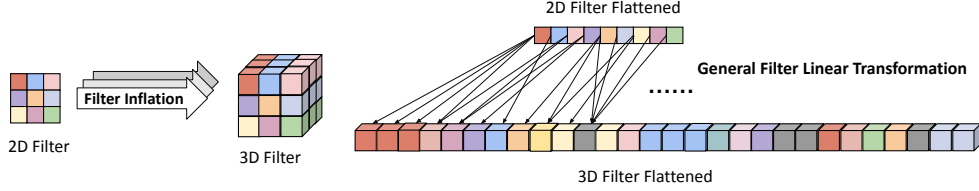


Figure 2: The left figure shows the 2D convolution and the converted 3D convolution by directly copying the 2D filter. The right figure shows a general filter transformation, in which 2D filters are linearly transformed into 3D filters.

represented as a 4D tensor of shape  $[M, N, K, K]$ , representing output dimension, input dimension, and two spatial kernel sizes, respectively. A 3D convolutional filter has an extra dimension and its shape is  $[M, N, K, K, K]$ . To better illustrate this point, we ignore the output and input dimensions and only consider a spatial slice of the 2D filter with shape  $[K, K]$ . The simplest way to convert this 2D filter to 3D is to copy the 2D filter and repeat it by  $K$  times along a third dimension, as illustrated in Fig. 2. This operation is the same as the *inflation* trick used by [62] to initialize a video model with a pretrained 2D ConvNet. More generally, if we represent the original 2D filter slice as a vector with  $K^2$  elements and the 3D filter slice as a vector with  $K^3$  elements, this inflation can be represented by a linear transformation matrix  $\mathbf{T}$  with shape  $K^2 \times K^3$ . This transformation matrix can represent handcrafted operations such as inflation along different orientations, rotations, and can also be trained. We will discuss how this transformation matrix  $\mathbf{T}$  impacts the transfer performance in Section 4.8.

Besides convolution, other operations such as downsampling, batch normalization (BN), nonlinear activation can be easily migrated to 3D. Our 3D model inherits the architecture of the original 2D ConvNet, but we also add an input layer with 3 convolutional layers, and an output layer depending on the target task. For classification, we use a global average pooling followed by two fully connected layers to get the final prediction. For semantic segmentation, the output layer is a U-Net style decoder [65]. The architecture of the input/output layers are described in more detail in Section 6.4.

## 4 Empirical Evaluation

To study the image to point-cloud transfer, we formulate eight questions and provide experimental results to address these questions. These questions are organized in three parts: (i) Can we use transferred image models to understand point-clouds? (Section 4.1, Section 4.2, Section 4.3) (ii) How do different factors such as point-cloud processing methods, pretrained image datasets, and types of tasks, impact the transferring performance? (Section 4.4, Section 4.5, Section 4.6, Section 4.7) (iii) How can we further improve the transferring performance? (Section 4.8)

**Datasets.** We benchmark the transferred models on ModelNet 3D Warehouse classification [8], S3DIS indoor segmentation [4], and SemanticKITTI outdoor segmentation [1] tasks. ModelNet 3D Warehouse is a CAD model classification dataset that consists of point-clouds with 40 categories. CAD models in this benchmark come from 3D Warehouse [7]. In this benchmark, we only utilize the x, y, z coordinates as features. S3DIS is an indoor dataset collected from real-world indoor scenes and includes 3D scans of Matterport Scanners from 6 areas. It provides point-wise annotations for indoor objects like chair, table, and bookshelf, *etc.* SemanticKITTI dataset from KITTI Vision Odometry [66] is a driving scene dataset. It provides dense point-wise annotations for the complete 360 degrees field-of-view of the deployed automotive lidar, which is currently one of the most challenging datasets.

We use pretrained ResNet [67] as 2D ConvNets mostly throughout our experiments. Depending on the experiments, ResNets are pretrained on Tiny-ImageNet, ImageNet-1K, ImageNet-21K [68], Cityscapes [69], ADE20K [70], and Fractal database (FractalDB) [48]. Our pretrained models are directly downloaded from various sources, with detailed links provided in Section 6.1.

#### 4.1 Can we use transferred image models to understand point-clouds?

To evaluate the feasibility of transferring pretrained 2D image models to 3D point-cloud tasks, we use a ResNet-18 model which is pretrained on ImageNet-1K. We convert 2D ConvNets into 3D ConvNets using the procedure described in Section 3. We hypothesize that, if a pretrained 2D image model is capable of understanding point-clouds directly, we can see an acceptable performance by only finetuning input and output layers of the transferred model. To further our hypothesis, we believe that, as we gradually relaxing the freezing parameters—finetuning BN parameters as well, the transferred model can achieve better performance, even surpassing training-from-scratch performance. Thus, in this first experiment, we propose four different settings, as shown in Table 1: 1) In the first setting, we only finetune the input (**I**) and output (**O**) layers; 2) In addition to **I**, **O**, we also allow the BN layers to update the mean ( $\mu$ ) and variance ( $\sigma$ ) based on the input data; 3) In the third setting, we include all the previous relaxation of constraints **I**, **O**,  $\mu$ ,  $\sigma$ , and also finetune BN weight (**W**) and bias (**b**); 4) finetune the whole network.

Table 1: Transfer experiments from pretrained **ResNet-18** on ImageNet-1K to ModelNet 3D Warehouse (ModelNet40), S3DIS (area 5), and SemanticKITTI (val set), respectively. We list some well-known point-cloud benchmarks in the third group for easy comparison to prior arts. † means our reproduced results based on their official code since they do not provide the results on these evaluation.

Layers to finetune	ModelNet(top 1 Acc%)	S3DIS(mIoU%)	SemanticKITTI(mIoU%)
I, O	78.69	53.54	55.78
I, O, $\mu$ , $\sigma$	83.45	54.86	56.29
I, O, $\mu$ , $\sigma$ , W, b	88.09	55.22	58.76
whole network	89.14	56.62	65.59
from scratch	88.61	55.09	64.75
linear I, O	69.74	48.83	54.43
linear network(w/o backbone)	8.91	-	-
from scratch (linear I, O)	88.53	54.79	64.01
3DShapeNets [8]	77.0	-	-
DeepPano [9]	77.63	-	-
Xu <i>et al.</i> [71]	81.26	-	-
PointNet [30]	89.2	42.97	17.4†
PointNet++ [31]	90.7	50.73†	22.1†
DGCNN [72]	90.7	47.94	-
RSNet [73]	-	51.93	-
SPGraph [74]	-	58.04	20.00 (test)
TangentConv [75]	-	52.6	35.9 (test)
SqueezeSegV3 [22]	-	-	57.31 †

We discover that even if we **only finetune the input/output layers** while keep the image representation untouched, **the transferred model achieves highly competitive performance**, outperforming a large number of task-specific models on all three benchmarks. Specifically, it outperforms 3D ShapeNet [8] and DeepPano [9] by 1.69% and 1.06% which were the state-of-the-arts in year 2015, respectively, in top 1 accuracy on the ModelNet 3D Warehouse dataset. For the more challenging segmentation task on the S3DIS and SemanticKITTI dataset, the minimal transferred model outperforms a wide range of state-of-the-arts [30, 31, 72, 74, 75]. It even approaches the performance of SqueezeSegV3 [23] (only 1.53 points mIoU lower), a task-specific network customized for driving scene segmentation.

We then **finetune the BN weight and bias** but do not change weights of the pretrained model, **the performance can be further improved**. Specifically, it is largely improved by 9.4% accuracy on ModelNet 3D Warehouse. Compared with training from scratch, the performance does not drop by a big margin: 0.52% accuracy and 5.99% mIoU on the ModelNet and SemanticKITTI.

To quantify the representation ability of the transformed 3D ConvNets for point-cloud, we refer to previous works for the method of finetuning only the simplest linear input layer and a linear classifier [12, 11, 46]. Thus, we design the simplest linear input and output layers for classification and segmentation task, as shown in Section 6.4. We compare the results Table 1 with two baseline

Table 2: The performance of pretrained PointNet++ on Tiny-ImageNet and HRNetV2-W48 on Cityscapes transferring to ModelNet 3D Warehouse and SemanticKITTI for classification and segmentation.

Layers to finetune	Tiny-ImageNet $\rightarrow$ ModelNet	Cityscapes $\rightarrow$ SemanticKITTI
	PointNet++ (Cls top 1 Acc%)	HRNetV2-W48 (Seg mIoU%)
I, O, $\mu$ , $\sigma$	82.34	36.04
whole network	90.72	49.37
from scratch	90.67	44.12

settings: 1) stacking the input and output layer to form a network (linear network (w/o backbone)). We increase the output channel of the input layer equal to the input channel of the output layer; 2) training this new architecture from scratch (from scratch (linear I, O)).

We observe that compared with the **linear network formed by linear input and output layer**, the introduced 3D ConvNet transformed from the pretrained 2D ConvNet **provides effective representations that improves performance from 8.91% to 69.74%**. Even compared with previous works [31, 72, 74], the simplest transferred model still outperforms them on the S3DIS and SemanticKITTI.

**With finetuning the whole network**, the transformed ConvNets **steadily outperform** training from scratch, over 0.53% accuracy, 1.53% mIoU, and 0.84% mIoU on the ModelNet, S3DIS, and SemanticKITTI dataset, respectively. However, improvements are not a large margin, and it is a limitation which we will explore in the future.

Therefore, we conclude that pretrained 2D image models can provide a good representation for 3D point-clouds, and more importantly, it can indeed transfer to 3D point-cloud tasks.

#### 4.2 Can image pretraining help projection-based and point-based models?

The above experiments are conducted on the 3D sparse convolution-based model. We are driven to explore if image pretraining also help projection-based and point-based models, as they are widely used for point-cloud understanding.

We choose the typical point-based model, PointNet++ [31], and train it on the Tiny-ImageNet dataset. Training detail is in Section 6.1. As shown in Table 2, after pretraining on Tiny-ImageNet, we finetune it on ModelNet 3D Warehouse. We observe that, if only finetuning the input/output layers and adapting BN mean and variance, the transferred model achieves 82.34% top 1 accuracy on ModelNet 3D Warehouse. When finetuning the whole network, the performance is slightly better than training from scratch.

For the projection-based method, we choose HRNet [76] as the starting point. We use a HRNetV2-W48 pretrained on Cityscapes, then finetune it on SemanticKITTI. As shown in Table 2, finetuning input/output layers and updating mean and variance yields an accuracy of 36.04%. Further finetuning the entire network improve the accuracy to 49.37 %, > 5% mIoU higher than training from scratch.

Therefore, the experiment demonstrates that image pretraining is also effective for point-based model and projection-based model.

#### 4.3 Can transferred model improve data efficiency?

Table 3: The performance of **ResNet-50** training on ModelNet 3D Warehouse with 1%, 5%, 10% randomly selected data.

	1% train data	5% train data	10% train data	100% train data
w/ pretraining	24.92	71.11	76.82	88.90
w/o pretraining	13.66	68.56	74.31	88.53

Obtaining and annotating point-cloud data is much more difficult and expensive than images. Thus, we want to explore if transferring image models to 3D can help improve data efficiency.

To investigate this question, we transfer a ResNet-50 pretrained on ImageNet-1K to 3D and finetune the entire model on the ModelNet 3D Warehouse using randomly sampled 1%, 5%, 10% training data. We observe that image-pretrained models steadily outperform models trained from scratch. Especially for the most difficult setting with 1% training data, the performance is improved by 11.26% accuracy. As for the 5% and 10% training data, the transformed networks outperform 2.55% and 2.51% top 1 accuracy, respectively. This result shows that models pretrained on images can significantly improve data efficiency, especially on the extremely low data regime. However, we observe that the benefit becomes marginal as we have more training data.

#### 4.4 How does the scale of image dataset affect performance?

We next explore how the performance of transferring changes as the scale of image dataset changes. Here, we control for the size of image dataset: we use ResNet-50 pretrained on Tiny-ImageNet, ImageNet-1K, and ImageNet-21K. In particular, Tiny-ImageNet has 100,000 images across 200 classes, ImageNet-1K was created by selecting a subset of 1.2M images from the full ImageNet dataset, and ImageNet-21K is the full ImageNet dataset with 14,197,122 images and 21,841 labels. We here utilize ResNet-50 as our backbone since rich pretrained models are based on it. The more details are in the Section 6.1.

As the scale of pretrained dataset increasing from 100,000 to 1,200,00, the performance improves significantly as shown in Table 4. In particular, with only finetuning the input (I) and output (O) layers, pretraining on ImageNet-1K outperforms pretraining on Tiny-ImageNet by 15.07%. When dataset size increases from 1.2M to 14M, we discover a slight drop when we only train the input and output layers. If we train the whole normalization layer, the performance increases compare to pretraining on a smaller size. The *hypothesis* is that, as the scale of the data increases, the distribution variance increases, making the gap between point-clouds and images larger. Thus, effective representations learned from images decline. However, as we finetuning normalization layers, the distribution variances are mitigated [77].

With full network finetuning, the final accuracy is around 0.5% higher than training from scratch. Scaling up the size of pretraining dataset does not bring notable improvement. This result is contradicting many observations in image-to-image transfer tasks. Therefore, we conclude that the performance of the transferred model cannot fully scale up as the scale of image dataset increases.

#### 4.5 How does the type of image dataset affect performance?

We then conduct experiments on FractalDB dataset [48] to explore how the type of image dataset affects the transferring performance. In particular, FractalDB dataset is a large-scale dataset with 1M non-natural images and 1K/10K categories (FractalDB1K/10K) generated by computer.

We surprisingly discover that such a non-natural image pretraining can significantly help point-cloud classification. With only finetuning the input and output layers, the performance is even better than the transferred model pretrained on ImageNet. It achieves at least 2.07% accuracy improvement when using FractalDB1K for pretraining compared with pretraining on ImageNet. We also discover that updating the mean and variance harms the transfer performance significantly by up to 13 % accuracy. This is surprising since in all other experiments, updating BN mean and variance almost always improves the performance. When finetuning more parameters (I, O,  $\mu$ ,  $\sigma$ , W, b), the performance can be improved by 15.64% and 10.37% top 1 accuracy for the models pretrained on FractalDB1K and FractalDB10K, respectively.

Therefore, we conclude that different types of image data do make a difference to the transfer performance and surprisingly, non-natural images like FractalDB are more effective than natural images when finetuning only input and output layers.

#### 4.6 How does the image task affect performance?

The above pretraining is mainly from the classification task. To explore the effect of pretraining on different tasks, we pretrain ResNet-18 on the segmentation task of Cityscapes [69] and ADE20K [70] dataset. For a fair comparison with pretraining on ImageNet-1K, we only load the encoder part.

The experiment results in Table 5 shows that pretraining on Cityscapes significantly improves the performance over pretraining on ImageNet-1K when transferring to SemanticKITTI. If only finetuning

Table 4: The transferring classification performance of **ResNet-50** from Tiny-ImageNet, ImageNet-1K, ImageNet-21K, Fractal1K and Fractal10K to ModelNet 3D Warehouse.

Layers to finetune	Tiny-ImageNet	ImageNet-1K	ImageNet-21K	FractalDB1k	FractalDB10k
	ModelNet (top 1 Acc.%)			ModelNet (top 1 Acc.%)	
I, O	68.40	83.47	81.81	85.54	83.55
I, O, $\mu$ , $\sigma$	81.69	83.28	82.10	72.53	77.96
I, O, $\mu$ , $\sigma$ , W, b	88.70	88.98	89.18	88.17	88.33
whole network	89.06	88.90	89.19	88.45	88.49
from scratch	88.53			88.53	

Table 5: The performance of **ResNet-18** pretrained from image semantic segmentation transferring to point-cloud segmentation. We compare the pretrain on Cityscapes and ADE20K with pretrain on ImageNet-1K for transferring to SemanticKITTI and S3DIS respectively.

Layers to finetune	ImageNet-1K	Cityscapes	ImageNet-1K	ADE20K
	SemanticKITTI (mIoU%)		S3DIS (mIoU%)	
I, O	55.78	58.48	53.54	55.28
I, O, $\mu$ , $\sigma$	56.29	56.71	54.86	54.95
I, O, $\mu$ , $\sigma$ , W, b	58.76	59.54	55.22	55.28
whole network	65.59	65.55	56.62	56.11
from scratch	64.75		55.09	

the input and output layers, there is a 2.70% mIoU improvement. The result shows representations learned from Cityscapes is more suitable than those learned from ImageNet-1K for SemanticKITTI segmentation. For pretraining from ADE20K and pretraining from ImageNet-1K to ModelNet 3D Warehouse, the transferred model exhibits comparable results. One possible explanation is that the S3DIS dataset is closer to the image dataset since it consists of RGB features.

Therefore, we conclude that pretraining image task can affect the performance. As the task becomes closer to the target task, the performance improves.

#### 4.7 How do better image models affect performance?

We then explore whether different 2D models on image tasks affect the performance of transferring to point-cloud tasks. Specifically, we conduct experiments on ModelNet 3D Warehouse, on top of pretrained ResNet-18, ResNet-50, and ResNet-152 on ImageNet-1K, as shown in Table 6.

Table 6: The performance of pretrained models on ImageNet-1K transfer to ModelNet 3D Warehouse.

Layers to finetune	ResNet-18	ResNet-50	ResNet-152
I, O	78.69	83.47	69.33
I, O, $\mu$ , $\sigma$	83.45	83.28	81.68
I, O, $\mu$ , $\sigma$ , W, b	88.09	88.98	88.66
whole network	89.14	88.90	88.45
from scratch	88.61	88.53	88.74

We observe that, for the setting of only finetuning the input and output layers, the performance on ModelNet 3D Warehouse can be improved by 4.78% as the backbone is scaled from ResNet-18 into ResNet-50. However, we observe that using ResNet-152 lead to a noticeable performance drop by 14.14%. Our *hypothesis* is that the error brought by the data distribution gap between image and point-cloud gradually accumulates as the number of layers increases. Therefore, only training the input and output layers can hardly transfer the good representation from image to point-cloud. This issue can be alleviated by updating the BN mean and variance, which helps to shift the distribution from different domain [77]. Thus, we can observe the performance is largely improved by 12.35%



Table 7: The performance of different filter inflation based on **ResNet-18** on the ModelNet 3D Warehouse dataset. T1, T2 and T3 are handcraft designed filter inflation. The ST (Shared T) denotes we learn a filter transformation for all convolutions, and the NST (Non-shared T) denotes we learn a filter transformation for each convolution. RI means that we use random initialization.

Layers to finetune	T1	T2	T3	ST	NST	ST(RI)	NST(RI)
I, O, $\mu$ , $\sigma$	82.21	81.81	82.25	84.36	87.24	84.40	86.35

when updating the mean and variance. Furthermore, when further training the weight and bias in the normalization layer, the distribution shift can be further mitigated.

Meanwhile, as finetuning the whole network, the performance is not improved as the scale of models increases, which is also a limitation. We conclude that better image models cannot entirely improve performance.

#### 4.8 How to design the filter transformation?

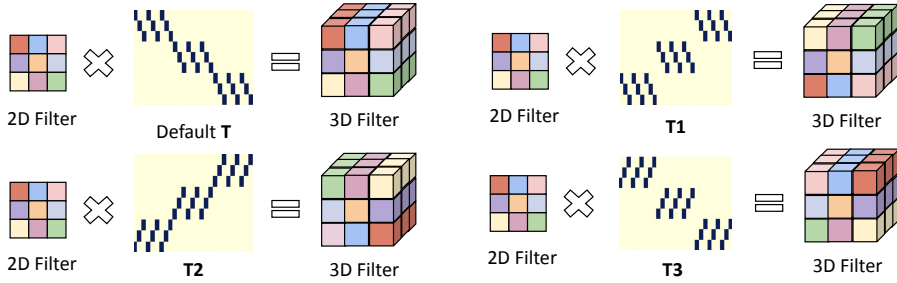


Figure 3: Visual examples for handcraft designed filter transformation.

In the above experiments, we use filter inflation, *i.e.*, directly copy the 2D filter  $K$  times into 3D, which can actually be formed as a filter transformation, as shown in the top left of Fig. 3. This motivates us to think about how to design a better filter transformation.

We first design three handcrafted filter transformation **T1**, **T2**, **T3**, which copies 2D weights along different orientations, as shown in Fig. 3. Then we try to directly learn the filter transformation **T** instead of handcrafted design. We consider two settings: 1) all 2D filters share the same learnable filter transformation, 2) each 2D filter has its own learnable filter transformation. To learn such filter transformation, we fix the weight of the 2D filters, only train **T**, input, output layers, and update the mean and variance of BN. For the initialization of **T**, we consider initializing it by our default **T** and random initialization, respectively.

In Table 7, we observe that the performance is relatively stable for different handcraft designed filter inflation **T**. However, the performance is significantly improved by at least 4.99% top 1 accuracy, when using learnable transformation in a non-shared learning scheme initialized by the default **T**. For random initialization, the performance is also improved compared with the handcrafted design, although it is slightly worse than initialization by the default **T**.

Therefore, we conclude that learnable filter transformation does perform better than handcrafted design. For learnable filters, however, initializing from handcrafted transformation outperforms random initialization.

## 5 Discussion, Limitation, and Conclusion

In this paper, we explore the feasibility of transferring the pretrained 2D ConvNets for performing 3D point-cloud tasks. Our experimental results in Section 4.1 show that visual representations pretrained on image datasets can indeed transfer to point-cloud. This is a surprising result, given that 2D images and 3D point-clouds represent visual information in highly different manners. Our *hypothesis* is: when we transfer 2D ConvNet pretrained on images to 3D, we essentially apply a linear projection

on the 2D convolutional filter; when processing 3D voxel input, this is equivalent to projecting 3D input to 2D first, and then process the input with trained 2D filters. This transferability reveals that 2D image features and 3D point-cloud features are closely correlated. In our future work, we plan to explore the reasons that we can transfer image models to point-cloud understanding.

We also explore factors that impact the transferring performance. The transfer performance is surprisingly good if we only finetune minimal parts of the model, but if we finetune the entire model and compare with training the model from scratch, we do not observe significant benefits. We seek to improve this by checking the impact of image dataset scale, type, pretraining tasks, and scale of the pretrained image model. However, after the exploration, we still only observe limited improvements. Given the fast progress of image representation learning, the abundance of image data, and the difficulty of obtaining point-cloud data, we believe there is huge potential for further exploring how to transfer image models to point-cloud understanding for a better performance and data efficiency. This will also be a focus of our future work.

Although the performance is limited, our results still show a very promising direction—design better filter transformation, use more suitable datasets and models. Compared with previous works that seek improvements from the aspect of designing architectures and pretraining only on the point-cloud modality, our work is not limited by the immature representation learning scheme, small scale point-cloud dataset, and expensive pretraining cost. We believe that image pretraining is one of the solutions to the bottleneck of point-cloud understanding and do hope this direction can inspire the research community in the future.

## References

- [1] J. Behley, M. Garbade, A. Milioto, J. Quenzel, S. Behnke, C. Stachniss, and J. Gall. SemanticKITTI: A Dataset for Semantic Scene Understanding of LiDAR Sequences. In *Proc. of the IEEE/CVF International Conf. on Computer Vision (ICCV)*, 2019.
- [2] Holger Caesar, Varun Bankiti, Alex H Lang, Sourabh Vora, Venice Erin Liong, Qiang Xu, Anush Krishnan, Yu Pan, Giancarlo Baldan, and Oscar Beijbom. nuscenes: A multimodal dataset for autonomous driving. In *Proceedings of the IEEE/CVF conference on computer vision and pattern recognition*, pages 11621–11631, 2020.
- [3] Xiangyu Yue, Bichen Wu, Sanjit A Seshia, Kurt Keutzer, and Alberto L Sangiovanni-Vincentelli. A lidar point cloud generator: from a virtual world to autonomous driving. In *Proceedings of the 2018 ACM on International Conference on Multimedia Retrieval*, pages 458–464, 2018.
- [4] Iro Armeni, Sasha Sax, Amir R Zamir, and Silvio Savarese. Joint 2d-3d-semantic data for indoor scene understanding. *arXiv preprint arXiv:1702.01105*, 2017.
- [5] François Pomerleau, Francis Colas, and Roland Siegwart. A review of point cloud registration algorithms for mobile robotics. *Foundations and Trends in Robotics*, 4(1):1–104, 2015.
- [6] Chenfeng Xu, Bohan Zhai, Bichen Wu, Tian Li, Wei Zhan, Peter Vajda, Kurt Keutzer, and Masayoshi Tomizuka. You only group once: Efficient point-cloud processing with token representation and relation inference module, 2021.
- [7] Sketchup. 3d modeling online freel3d warehouse models. <https://3dwarehouse.sketchup.com>, 2021.
- [8] Zhirong Wu, Shuran Song, Aditya Khosla, Fisher Yu, Linguang Zhang, Xiaoou Tang, and Jianxiong Xiao. 3d shapenets: A deep representation for volumetric shapes. In *Proceedings of the IEEE Conference on Computer Vision and Pattern Recognition (CVPR)*, June 2015.
- [9] Baoguang Shi, Song Bai, Zhichao Zhou, and Xiang Bai. Deeppano: Deep panoramic representation for 3-d shape recognition. *IEEE Signal Processing Letters*, 22(12):2339–2343, 2015.
- [10] Alexander Kolesnikov, Lucas Beyer, Xiaohua Zhai, Joan Puigcerver, Jessica Yung, Sylvain Gelly, and Neil Houlsby. Large scale learning of general visual representations for transfer. *arXiv preprint arXiv:1912.11370*, 2019.
- [11] Ting Chen, Simon Kornblith, Mohammad Norouzi, and Geoffrey Hinton. A simple framework for contrastive learning of visual representations. In *International conference on machine learning*, pages 1597–1607. PMLR, 2020.

- [12] Kaiming He, Haoqi Fan, Yuxin Wu, Saining Xie, and Ross Girshick. Momentum contrast for unsupervised visual representation learning. In *Proceedings of the IEEE/CVF Conference on Computer Vision and Pattern Recognition*, pages 9729–9738, 2020.
- [13] Mathilde Caron, Hugo Touvron, Ishan Misra, Hervé Jégou, Julien Mairal, Piotr Bojanowski, and Armand Joulin. Emerging properties in self-supervised vision transformers. *arXiv preprint arXiv:2104.14294*, 2021.
- [14] Bernie Wang, Virginia Wu, Bichen Wu, and Kurt Keutzer. Latte: accelerating lidar point cloud annotation via sensor fusion, one-click annotation, and tracking. In *2019 IEEE Intelligent Transportation Systems Conference (ITSC)*, pages 265–272. IEEE, 2019.
- [15] Baoyuan Liu, Min Wang, Hassan Foroosh, Marshall Tappen, and Marianna Pensky. Sparse convolutional neural networks. In *Proceedings of the IEEE conference on computer vision and pattern recognition*, pages 806–814, 2015.
- [16] Christopher Choy, JunYoung Gwak, and Silvio Savarese. 4d spatio-temporal convnets: Minkowski convolutional neural networks. In *Proceedings of the IEEE Conference on Computer Vision and Pattern Recognition*, pages 3075–3084, 2019.
- [17] Haotian\* Tang, Zhijian\* Liu, Shengyu Zhao, Yujun Lin, Ji Lin, Hanrui Wang, and Song Han. Searching efficient 3d architectures with sparse point-voxel convolution. In *European Conference on Computer Vision*, 2020.
- [18] Hui Zhou, Xinge Zhu, Xiao Song, Yuexin Ma, Zhe Wang, Hongsheng Li, and Dahua Lin. Cylinder3d: An effective 3d framework for driving-scene lidar semantic segmentation. *arXiv preprint arXiv:2008.01550*, 2020.
- [19] Yan Yan, Yuxing Mao, and Bo Li. Second: Sparsely embedded convolutional detection. *Sensors*, 18(10):3337, 2018.
- [20] Zining Wang, Wei Zhan, and Masayoshi Tomizuka. Fusing bird’s eye view lidar point cloud and front view camera image for 3d object detection. In *2018 IEEE Intelligent Vehicles Symposium (IV)*, pages 1–6. IEEE, 2018.
- [21] Bichen Wu, Alvin Wan, Xiangyu Yue, and Kurt Keutzer. Squeezeseg: Convolutional neural nets with recurrent crf for real-time road-object segmentation from 3d lidar point cloud. In *ICRA*, 2018.
- [22] Bichen Wu, Xuanyu Zhou, Sicheng Zhao, Xiangyu Yue, and Kurt Keutzer. Squeezesegv2: Improved model structure and unsupervised domain adaptation for road-object segmentation from a lidar point cloud. In *ICRA*, 2019.
- [23] Chenfeng Xu, Bichen Wu, Zining Wang, Wei Zhan, Peter Vajda, Kurt Keutzer, and Masayoshi Tomizuka. Squeezesegv3: Spatially-adaptive convolution for efficient point-cloud segmentation. In *European Conference on Computer Vision*, pages 1–19. Springer, 2020.
- [24] Hang Su, Subhransu Maji, Evangelos Kalogerakis, and Erik Learned-Miller. Multi-view convolutional neural networks for 3d shape recognition. In *Proceedings of the IEEE international conference on computer vision*, pages 945–953, 2015.
- [25] Felix Järemo Lawin, Martin Danelljan, Patrik Tosteberg, Goutam Bhat, Fahad Shahbaz Khan, and Michael Felsberg. Deep projective 3d semantic segmentation. In *International Conference on Computer Analysis of Images and Patterns*, pages 95–107. Springer, 2017.
- [26] Alexandre Boulch, Bertrand Le Saux, and Nicolas Audebert. Unstructured point cloud semantic labeling using deep segmentation networks. *3DOR*, 2:7, 2017.
- [27] Bin Yang, Wenjie Luo, and Raquel Urtasun. Pixor: Real-time 3d object detection from point clouds. In *Proceedings of the IEEE conference on Computer Vision and Pattern Recognition*, pages 7652–7660, 2018.
- [28] Alex H Lang, Sourabh Vora, Holger Caesar, Lubing Zhou, Jiong Yang, and Oscar Beijbom. Pointpillars: Fast encoders for object detection from point clouds. In *Proceedings of the IEEE/CVF Conference on Computer Vision and Pattern Recognition*, pages 12697–12705, 2019.
- [29] Andres Milioto, Ignacio Vizzo, Jens Behley, and Cyrill Stachniss. Rangenet++: Fast and accurate lidar semantic segmentation. In *2019 IEEE/RSJ International Conference on Intelligent Robots and Systems (IROS)*, pages 4213–4220. IEEE, 2019.

- [30] Charles R. Qi, Hao Su, Kaichun Mo, and Leonidas J. Guibas. Pointnet: Deep learning on point sets for 3d classification and segmentation, 2016. cite arxiv:1612.00593.
- [31] Charles R Qi, Li Yi, Hao Su, and Leonidas J Guibas. Pointnet++: Deep hierarchical feature learning on point sets in a metric space. *arXiv preprint arXiv:1706.02413*, 2017.
- [32] Yangyan Li, Rui Bu, Mingchao Sun, Wei Wu, Xinhan Di, and Baoquan Chen. Pointcnn: Convolution on  $\chi$ -transformed points. In *Proceedings of the 32nd International Conference on Neural Information Processing Systems*, pages 828–838, 2018.
- [33] Binh-Son Hua, Minh-Khoi Tran, and Sai-Kit Yeung. Pointwise convolutional neural networks. In *Proceedings of the IEEE Conference on Computer Vision and Pattern Recognition*, pages 984–993, 2018.
- [34] Yongcheng Liu, Bin Fan, Gaofeng Meng, Jiwen Lu, Shiming Xiang, and Chunhong Pan. Densepoint: Learning densely contextual representation for efficient point cloud processing. In *Proceedings of the IEEE/CVF International Conference on Computer Vision*, pages 5239–5248, 2019.
- [35] Ze Liu, Han Hu, Yue Cao, Zheng Zhang, and Xin Tong. A closer look at local aggregation operators in point cloud analysis. In *European Conference on Computer Vision*, pages 326–342. Springer, 2020.
- [36] Peng-Shuai Wang, Yang Liu, Yu-Xiao Guo, Chun-Yu Sun, and Xin Tong. O-cnn: Octree-based convolutional neural networks for 3d shape analysis. *ACM Transactions on Graphics (TOG)*, 36(4):1–11, 2017.
- [37] Jiaxin Li, Ben M Chen, and Gim Hee Lee. So-net: Self-organizing network for point cloud analysis. In *Proceedings of the IEEE conference on computer vision and pattern recognition*, pages 9397–9406, 2018.
- [38] Artem Komarichev, Zichun Zhong, and Jing Hua. A-cnn: Annularly convolutional neural networks on point clouds. In *Proceedings of the IEEE/CVF Conference on Computer Vision and Pattern Recognition*, pages 7421–7430, 2019.
- [39] Di Feng, Yiyang Zhou, Chenfeng Xu, Masayoshi Tomizuka, and Wei Zhan. A simple and efficient multi-task network for 3d object detection and road understanding, 2021.
- [40] Alexey Dosovitskiy, Lucas Beyer, Alexander Kolesnikov, Dirk Weissenborn, Xiaohua Zhai, Thomas Unterthiner, Mostafa Dehghani, Matthias Minderer, Georg Heigold, Sylvain Gelly, et al. An image is worth 16x16 words: Transformers for image recognition at scale. *arXiv preprint arXiv:2010.11929*, 2020.
- [41] Ross Girshick, Jeff Donahue, Trevor Darrell, and Jitendra Malik. Rich feature hierarchies for accurate object detection and semantic segmentation. In *Proceedings of the IEEE conference on computer vision and pattern recognition*, pages 580–587, 2014.
- [42] Longlong Jing and Yingli Tian. Self-supervised visual feature learning with deep neural networks: A survey. *IEEE Transactions on Pattern Analysis and Machine Intelligence*, 2020.
- [43] Priya Goyal, Mathilde Caron, Benjamin Lefaudeaux, Min Xu, Pengchao Wang, Vivek Pai, Manat Singh, Vitaliy Liptchinsky, Ishan Misra, Armand Joulin, et al. Self-supervised pretraining of visual features in the wild. *arXiv preprint arXiv:2103.01988*, 2021.
- [44] Philip Bachman, R Devon Hjelm, and William Buchwalter. Learning representations by maximizing mutual information across views. *arXiv preprint arXiv:1906.00910*, 2019.
- [45] Mathilde Caron, Ishan Misra, Julien Mairal, Priya Goyal, Piotr Bojanowski, and Armand Joulin. Unsupervised learning of visual features by contrasting cluster assignments. *arXiv preprint arXiv:2006.09882*, 2020.
- [46] Xinlei Chen, Haoqi Fan, Ross Girshick, and Kaiming He. Improved baselines with momentum contrastive learning. *arXiv preprint arXiv:2003.04297*, 2020.
- [47] R Devon Hjelm, Alex Fedorov, Samuel Lavoie-Marchildon, Karan Grewal, Phil Bachman, Adam Trischler, and Yoshua Bengio. Learning deep representations by mutual information estimation and maximization. *arXiv preprint arXiv:1808.06670*, 2018.
- [48] Hirokatsu Kataoka, Kazushige Okayasu, Asato Matsumoto, Eisuke Yamagata, Ryosuke Yamada, Nakamasa Inoue, Akio Nakamura, and Yutaka Satoh. Pre-training without natural images. In *Proceedings of the Asian Conference on Computer Vision*, 2020.

- [49] Mathilde Caron, Piotr Bojanowski, Julien Mairal, and Armand Joulin. Unsupervised pre-training of image features on non-curved data. In *Proceedings of the IEEE/CVF International Conference on Computer Vision*, pages 2959–2968, 2019.
- [50] Ting Chen, Simon Kornblith, Kevin Swersky, Mohammad Norouzi, and Geoffrey Hinton. Big self-supervised models are strong semi-supervised learners. *arXiv preprint arXiv:2006.10029*, 2020.
- [51] Olivier Henaff. Data-efficient image recognition with contrastive predictive coding. In *International Conference on Machine Learning*, pages 4182–4192. PMLR, 2020.
- [52] Saining Xie, Jiatao Gu, Demi Guo, Charles R Qi, Leonidas Guibas, and Or Litany. Pointcontrast: Unsupervised pre-training for 3d point cloud understanding. In *European Conference on Computer Vision*, pages 574–591. Springer, 2020.
- [53] Xun Xu and Gim Hee Lee. Weakly supervised semantic point cloud segmentation: Towards 10x fewer labels. In *Proceedings of the IEEE/CVF Conference on Computer Vision and Pattern Recognition*, pages 13706–13715, 2020.
- [54] Ji Hou, Benjamin Graham, Matthias Nießner, and Saining Xie. Exploring data-efficient 3d scene understanding with contrastive scene contexts. *arXiv preprint arXiv:2012.09165*, 2020.
- [55] Zaiwei Zhang, Rohit Girdhar, Armand Joulin, and Ishan Misra. Self-supervised pretraining of 3d features on any point-cloud. *arXiv preprint arXiv:2101.02691*, 2021.
- [56] Angela Dai and Matthias Nießner. 3dmv: Joint 3d-multi-view prediction for 3d semantic scene segmentation. In *Proceedings of the European Conference on Computer Vision (ECCV)*, pages 452–468, 2018.
- [57] Zhengzhe Liu, Xiaojuan Qi, and Chi-Wing Fu. 3d-to-2d distillation for indoor scene parsing. *arXiv preprint arXiv:2104.02243*, 2021.
- [58] Maximilian Jaritz, Tuan-Hung Vu, Raoul de Charette, Emilie Wirbel, and Patrick Pérez. xmuda: Cross-modal unsupervised domain adaptation for 3d semantic segmentation. In *Proceedings of the IEEE/CVF Conference on Computer Vision and Pattern Recognition*, pages 12605–12614, 2020.
- [59] Yonglong Tian, Dilip Krishnan, and Phillip Isola. Contrastive representation distillation. *arXiv preprint arXiv:1910.10699*, 2019.
- [60] Ji Hou, Saining Xie, Benjamin Graham, Angela Dai, and Matthias Nießner. Pri3d: Can 3d priors help 2d representation learning? *arXiv preprint arXiv:2104.11225*, 2021.
- [61] Yueh-Cheng Liu, Yu-Kai Huang, Hung-Yueh Chiang, Hung-Ting Su, Zhe-Yu Liu, Chin-Tang Chen, Ching-Yu Tseng, and Winston H Hsu. Learning from 2d: Pixel-to-point knowledge transfer for 3d pretraining. *arXiv preprint arXiv:2104.04687*, 2021.
- [62] Joao Carreira and Andrew Zisserman. Quo vadis, action recognition? a new model and the kinetics dataset. In *proceedings of the IEEE Conference on Computer Vision and Pattern Recognition*, pages 6299–6308, 2017.
- [63] Hongming Shan, Yi Zhang, Qingsong Yang, Uwe Kruger, Mannudeep K Kalra, Ling Sun, Wenxiang Cong, and Ge Wang. 3-d convolutional encoder-decoder network for low-dose ct via transfer learning from a 2-d trained network. *IEEE transactions on medical imaging*, 37(6):1522–1534, 2018.
- [64] Kevin Lu, Aditya Grover, Pieter Abbeel, and Igor Mordatch. Pretrained transformers as universal computation engines. *arXiv preprint arXiv:2103.05247*, 2021.
- [65] Olaf Ronneberger, Philipp Fischer, and Thomas Brox. U-net: Convolutional networks for biomedical image segmentation. In *International Conference on Medical image computing and computer-assisted intervention*, pages 234–241. Springer, 2015.
- [66] A. Geiger, P. Lenz, and R. Urtasun. Are we ready for Autonomous Driving? The KITTI Vision Benchmark Suite. In *Proc. of the IEEE Conf. on Computer Vision and Pattern Recognition (CVPR)*, pages 3354–3361, 2012.
- [67] Kaiming He, Xiangyu Zhang, Shaoqing Ren, and Jian Sun. Deep residual learning for image recognition. In *Proceedings of the IEEE conference on computer vision and pattern recognition*, pages 770–778, 2016.

- [68] Jia Deng, Wei Dong, Richard Socher, Li-Jia Li, Kai Li, and Li Fei-Fei. Imagenet: A large-scale hierarchical image database. In *2009 IEEE conference on computer vision and pattern recognition*, pages 248–255. Ieee, 2009.
- [69] Marius Cordts, Mohamed Omran, Sebastian Ramos, Timo Rehfeld, Markus Enzweiler, Rodrigo Benenson, Uwe Franke, Stefan Roth, and Bernt Schiele. The cityscapes dataset for semantic urban scene understanding. In *Proceedings of the IEEE conference on computer vision and pattern recognition*, pages 3213–3223, 2016.
- [70] Bolei Zhou, Hang Zhao, Xavier Puig, Sanja Fidler, Adela Barriuso, and Antonio Torralba. Scene parsing through ade20k dataset. In *Proceedings of the IEEE conference on computer vision and pattern recognition*, pages 633–641, 2017.
- [71] Xu Xu and Sinisa Todorovic. Beam search for learning a deep convolutional neural network of 3d shapes. In *2016 23rd International Conference on Pattern Recognition (ICPR)*, pages 3506–3511. IEEE, 2016.
- [72] Yue Wang, Yongbin Sun, Ziwei Liu, Sanjay E Sarma, Michael M Bronstein, and Justin M Solomon. Dynamic graph cnn for learning on point clouds. *Acm Transactions On Graphics (tog)*, 38(5):1–12, 2019.
- [73] Qiangui Huang, Weiyue Wang, and Ulrich Neumann. Recurrent slice networks for 3d segmentation of point clouds. In *Proceedings of the IEEE Conference on Computer Vision and Pattern Recognition*, pages 2626–2635, 2018.
- [74] Loic Landrieu and Martin Simonovsky. Large-scale point cloud semantic segmentation with superpoint graphs. In *Proceedings of the IEEE Conference on Computer Vision and Pattern Recognition*, pages 4558–4567, 2018.
- [75] Maxim Tatarchenko, Jaesik Park, Vladlen Koltun, and Qian-Yi Zhou. Tangent convolutions for dense prediction in 3d. In *Proceedings of the IEEE Conference on Computer Vision and Pattern Recognition*, pages 3887–3896, 2018.
- [76] Ke Sun, Bin Xiao, Dong Liu, and Jingdong Wang. Deep high-resolution representation learning for human pose estimation. In *CVPR*, 2019.
- [77] Dequan Wang, Evan Shelhamer, Shaoteng Liu, Bruno Olshausen, and Trevor Darrell. Tent: Fully test-time adaptation by entropy minimization. In *International Conference on Learning Representations*, 2021.
- [78] Tal Ridnik, Emanuel Ben-Baruch, Asaf Noy, and Lihi Zelnik-Manor. Imagenet-21k pretraining for the masses, 2021.
- [79] Yifan Liu, Ke Chen, Chris Liu, Zengchang Qin, Zhenbo Luo, and Jingdong Wang. Structured knowledge distillation for semantic segmentation. In *Proceedings of the IEEE/CVF Conference on Computer Vision and Pattern Recognition*, pages 2604–2613, 2019.

## 6 Appendix

### 6.1 Implementation detail.

Our experiments are mainly conducted on ModelNet 3D Warehouse, S3DIS, and SemanticKITTI dataset. Specifically, as for the ModelNet 3D Warehouse dataset, all models that we use are trained on the train set of ModelNet 3D Warehouse and evaluated on the validation set. As for the S3DIS, all models that we use are trained on area 1, 2, 3, 4, 6 and evaluated on area 5. As for the SemanticKITTI dataset, all models are trained on splits 00-10 except 08 which is used for evaluation. For each of these datasets, all ResNet-series models are trained based on the same training scheme, and all experiments are implemented with Pytorch.

For the *ModelNet 3D Warehouse dataset*, during training, coordinates of point-cloud are randomly scaled, translated, and jittered. We use SGD optimizer with momentum 0.9, weight-decay  $10^{-4}$ , and initial learning rate 0.1 with cosine learning rate scheduler. Each mini batch is set to 32, and models are trained for 300 epochs. For both training and inference phase, we only utilize x, y, z coordinates without other features and set voxel size as 0.05. The experiments for ModelNet 3D Warehouse are all conducted on a Titan RTX GPU.

For the *S3DIS dataset*, during training, we concatenate all subparts of an indoor scene to train and validate on. Along x, y directions, scenes are randomly applied horizontal flip. RGB features are randomly jittered, translated, and auto contrasted. Finally, we normalize and clip point-clouds. We set voxel size as 0.05. We use SGD optimizer with momentum 0.9, weight-decay  $10^{-4}$ , and initial learning rate 0.1 with polynomial learning rate scheduler. Each mini batch is set to 3, and models are trained for 400 epochs. The experiments for S3DIS are all conducted on 2 Titan RTX GPUs.

For the *SemanticKITTI dataset*, during training, coordinates of each point-cloud are randomly scaled and rotated. We use SGD optimizer with momentum 0.9, weight-decay  $10^{-4}$ , and initial learning rate 0.24 with cosine warmup learning rate scheduler. Each mini batch is set to 2, and models are trained for 15 epochs. For both training and inference phase, we utilize x, y, z coordinates as well as intensity feature and set voxel size as 0.05. The experiments for SemanticKITTI are all conducted on 4 Titan RTX GPUs.

Most of our pretrained models come from open-sources,<sup>2 3 4 5 6 7</sup>, so we do not need to take time and computational resources for pretraining. We use torchsparse<sup>8</sup> to produce sparse 3D convolutions.

**Detail of Section 4.1.** All the experiments in this section are conducted based on pretrained ResNet18 on ImageNet1K from Pytorch. The results in the first group of Table. 1 are based on our default ResNet, as shown in the Section 6.4 listing 3 and 4. The results in the second group of Table. 1 are based on ResNet with linear input and output layer, as shown in the Section 6.4 listing 5 and 6. In detail, the pseudo code of linear network (w/o backbone) is shown below.

```
1 Class linear_net(nn.Module):
2     def __init__(self):
3         super().__init__()
4         self.input_layer = nn.Sequential(
5             sparse_conv3d(input_dim, layer4_0dim, k=3, s=1),
6             sparse_bn(layer1_1dim))
7         self.output_layer = nn.Sequential(
8             global_average_pooling,
9             nn.Linear(layer4_0dim, class_num),
10            nn.bn(class_num))
11     def forward(self, x):
12         x = self.input_layer(x)
```

<sup>2</sup><https://pytorch.org/vision/stable/models.html>

<sup>3</sup><https://github.com/Alibaba-MIIL/ImageNet21K>

<sup>4</sup>[https://github.com/irfanICMLL/structure\\_knowledge\\_distillation](https://github.com/irfanICMLL/structure_knowledge_distillation)

<sup>5</sup><https://github.com/CSAILVision/semantic-segmentation-pytorch>

<sup>6</sup><https://github.com/hiroakatsukataoka16/FractalDB-Pretrained-ResNet-PyTorch>

<sup>7</sup><https://github.com/HRNet/HRNet-Semantic-Segmentation/tree/pytorch-v1.1>

<sup>8</sup><https://github.com/mit-han-lab/torchsparse>

```
13         return self.output_layer(x)
```

Listing 1: Pseudo code of linear network without backbone

**Detail of Section 4.2.** For the pretraining of PointNet++ on Tiny-ImageNet dataset, we treat each pixel of a image as a point. We use the original pixel location as  $x$  and  $y$  coordinates of the corresponding point and append all points with  $z$  equal to 1. Then, we use the PointNet-SSG version, for each set abstraction module [31], points are sampled into  $1/4$ . We choose query ball grouping mechanism and set radius as 3. Then, we use SGD optimizer with momentum 0.9, weight decay  $10^{-4}$ , and initial learning rate 0.1 with decay rate 0.1 per 30 epochs. We set batch size to 64 and train the PointNet++ on two Titan RTX GPUS for 90 epochs.

As for the training phase on the ModelNet 3D Warehouse dataset, we use Adam optimizer with 0.001 learning rate for both training from scratch and finetuning schemes. Batch size is set to 32. We train the model for 200 epochs on one Titan RTX GPU.

We directly use the pretrained HRNet from the official code [76]. Specifically, we choose to use the official code of SqueezeSegV3 [23] as our base code. We substitute SqueezeSegV3 backbone with HRNetV2-W48, and all the other training schemes are totally kept the same.

**Detail of Section 4.3.** The pretrained ResNet50 on ImageNet1K also comes from Pytorch. Both the training from scratch and the finetuning models use the same selected training set and are evaluated on the whole validation set of ModelNet 3D Warehouse.

**Detail of Section 4.4, Section 4.5, Section 4.6, Section 4.7.** The pretrained ResNet50 on Tiny-ImageNet is trained by ourselves since there is rarely such pretrained model. The training scheme is directly from Pytorch provided code<sup>9</sup>. The pretrained ResNet50 on ImageNet1K is from Pytorch, and the pretrained ResNet50 on ImageNet21K is from recent work [78]. The pretrained ResNet50 on both FractalDB1K and FracatalDB10K are from the official code of [48]. The pretrained ResNet18 on Cityscapes is from [79], and the pretrained ResNet18 on ADE20K is from [70]. The pretrained ResNet18, ResNet50, ResNet152 are from Pytorch pretrained models. All the finetuning schemes in these experiments are as same as above illustrated ModelNet 3D Warehouse training scheme without any changes.

**Detail of Section 4.8.** The implementation pseudo code of a 3D sparse convolution with learnable  $T$  is shown below.

```
1 import torchsparse.nn.functional as spf
2 import torch.nn as nn
3 class conv3dwithT(nn.Module):
4     def __init__(self):
5         super().__init__()
6         self.filter_trans = nn.Parameter(torch.zeros(K^2, K^3))
7         init_(self.filter_trans)
8
9     def forward(self, x, pre_conv2d):
10         #input x is the feature, and the pre_conv2d is the pretrained
11         #2D weight
12         Cout, Cin, K, K = pre_conv2d.shape
13         conv3d_kernel = torch.matmul(pre_conv2d.view(Cout, Cin, -1),
14                                     self.filter_trans)
15         return spf.sparse_conv3D(x, conv3d_kernel)
```

Listing 2: Pseudo code of 3D sparse convolution with learnable  $T$

For shared filter transformation, all pretrained 2D convolution weights are multiplied by the same learnable filter transformation. For non-shared filter transformation, each pretrained 2D convolution weight is multiplied by its own filter transformation.

## 6.2 Detail illustration of our hypothesis Section 5.

In our discussion section, we provide a hypothesis about why pretrained 2D ConvNets can be used in 3D point-cloud. A further illustration is shown in Fig. 4.

<sup>9</sup><https://github.com/pytorch/examples/tree/cbb760d5e50a03df667cdc32a61f75ac28e11cbf/imagenet>



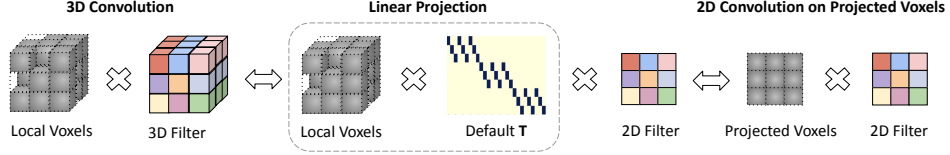


Figure 4: Visualization of our hypothesis. We hypothesize that directly performing 3D convolution on local voxels is similar to first projecting local voxels to 2D, then applying 2D convolution on projected voxels.

Although the above visual example applies to our default  $\mathbf{T}$ , which means directly copy 2D filters, it can actually be more general as  $\mathbf{T}$  can be any transformation matrix.

### 6.3 Visualization examples of learned filter transformation.

In Section 4.8, we discuss that, besides handcrafted filter transformations, there are also learned filter transformations. When all convolution layers share one common  $\mathbf{T}$ , performance increases compared to handcrafted  $\mathbf{T}$ , and non-shared filter transformations are more so. Here, we provide 2 visualizations showing shared and non-shared  $\mathbf{T}$ , initialized using default  $\mathbf{T}$  and randomly.

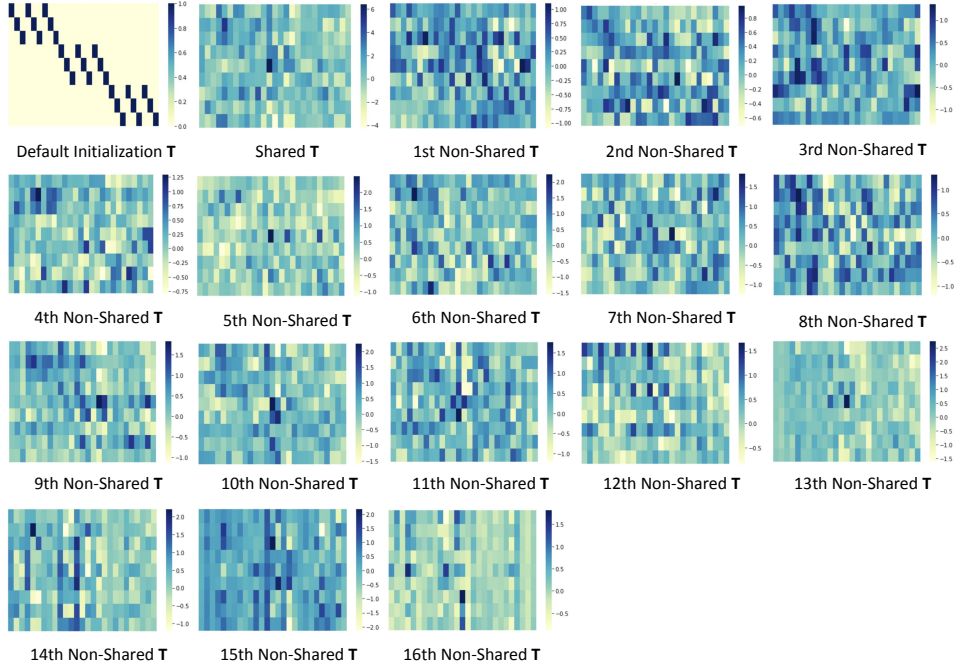


Figure 5: Visual examples for filter transformation, initialized by default  $\mathbf{T}$ . The first sub-figure is initialization  $\mathbf{T}$  for both the shared and non-shared filter transformation. The second sub-figure is shared  $\mathbf{T}$ . The rest of sub-figures belong to each convolution layer when filter transformations are non-shared.

### 6.4 Details of used Architectures.

```

1 Class Default_3DRes_cls(nn.Module):
2     def __init__(self, res_block):
3         super().__init__()
4         # res_block means the residual block as same as the
          conventional ResNet.
5         self.input_layer = nn.Sequential(
6             sparse_conv3d(input_dim, layer1_idim, k=3, s=1),

```

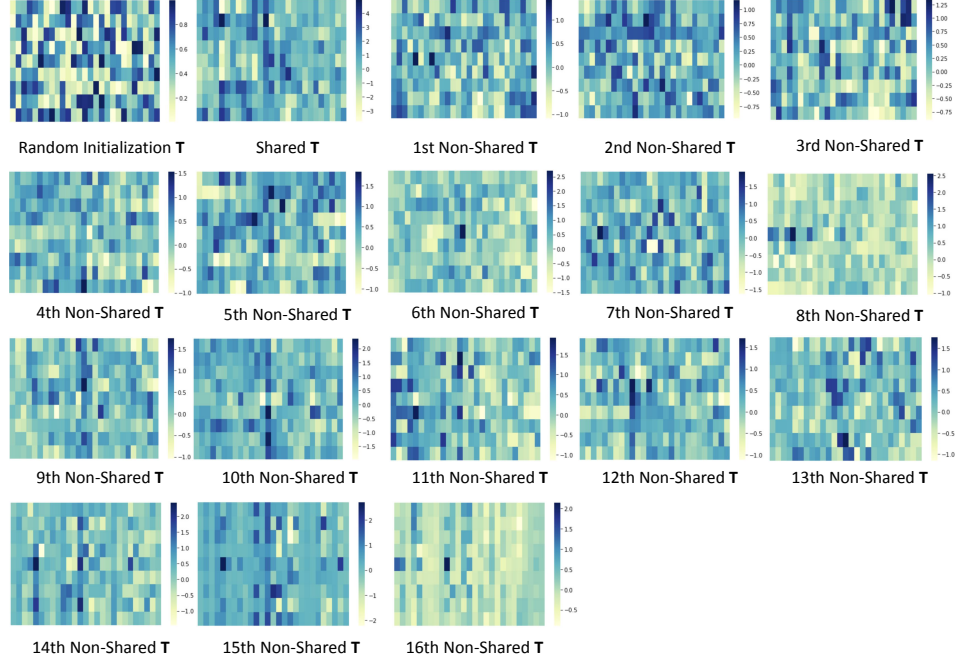


Figure 6: Visual examples for filter transformation, initialized by random  $\mathbf{T}$ . The first sub-figure is initialization  $\mathbf{T}$  for both the shared and non-shared filter transformation. The second sub-figure is shared  $\mathbf{T}$ . The rest of sub-figures belongs to each convolution layer when filter transformations are non-shared.

```

7         sparse_bn(layer1_Idim),
8         sparse_ReLU(True),
9         sparse_conv3d(layer1_Idim, layer1_Idim, k=3, s=1),
10        sparse_bn(layer1_Idim),
11        sparse_ReLU(True),
12        sparse_conv3d(layer1_Idim, layer1_Idim, k=3, s=2),
13        sparse_bn(layer1_Idim),
14        sparse_ReLU(True))
15
16        self.layer1 = inflated_resnet_layer1(res_block, layer1_Idim,
17        layer1_0dim)
18        self.layer2 = inflated_resnet_layer2(res_block, layer2_Idim,
19        layer2_0dim)
20        self.layer3 = inflated_resnet_layer3(res_block, layer3_Idim,
21        layer3_0dim)
22        self.layer4 = inflated_resnet_layer4(res_block, layer4_Idim,
23        layer4_0dim)
24
25        self.output_layer = nn.Sequential(
26            global_average_pooling,
27            nn.Linear(layer4_0dim, 1024),
28            nn.bn(1024),
29            nn.ReLU(True),
30            nn.Linear(1024, class_num),)
31
32    def forward(self, x):
33        x = self.input_layer(x)
34        x = self.layer1(x)
35        x = self.layer2(x)
36        x = self.layer3(x)
37        x = self.layer4(x)

```

```
34         return self.output_layer(x)
```

Listing 3: Pseudo code of inflated ResNet for classification

```
1 Class Default_3DRes_seg(nn.Module):
2     def __init__(self, res_block):
3         super().__init__()
4         # res_block means the residual block as same as the
         conventional ResNet.
5         self.input_layer = nn.Sequential(
6             sparse_conv3d(input_dim, layer1_Idim, k=3, s=1),
7             sparse_bn(layer1_Idim),
8             sparse_ReLU(True),
9             sparse_conv3d(layer1_Idim, layer1_Idim, k=3, s=1),
10            sparse_bn(layer1_Idim),
11            sparse_ReLU(True),
12            sparse_conv3d(layer1_Idim, layer1_Idim, k=3, s=2),
13            sparse_bn(layer1_Idim),
14            sparse_ReLU(True))
15
16        self.layer1 = inflated_resnet_layer1(res_block, layer1_Idim,
layer1_0dim)
17        self.layer2 = inflated_resnet_layer2(res_block, layer2_Idim,
layer2_0dim)
18        self.layer3 = inflated_resnet_layer3(res_block, layer3_Idim,
layer3_0dim)
19        self.layer4 = inflated_resnet_layer4(res_block, layer4_Idim,
layer4_0dim)
20
21        self.up1 = sparse_deconv(layer4_0dim, layer4_0dim, k=2, s=2),
self.decode1 = self.Sequential(
22            res_block(layer4_0dim+layer3_0dim, layer3_0dim),
23            res_block(layer3_0dim, layer3_0dim))
24
25
26        self.up2 = sparse_deconv(layer3_0dim, layer3_0dim, k=2, s=2)
self.decode2 = self.Sequential(
27            res_block(layer3_0dim+layer2_0dim, layer2_0dim),
28            res_block(layer2_0dim, layer2_0dim))
29
30
31        self.up3 = sparse_deconv(layer2_0dim, layer2_0dim, k=2, s=2)
self.decode3 = self.Sequential(
32            res_block(layer2_0dim+layer1_0dim, layer1_0dim),
33            res_block(layer1_0dim, layer1_0dim))
34
35
36        self.up4 = sparse_deconv(layer1_0dim, layer1_0dim, k=2, s=2)
self.decode4 = self.Sequential(
37            res_block(layer1_0dim+layer1_0dim, layer1_0dim),
38            res_block(layer1_0dim, layer1_0dim))
39
40
41        self.output_layer = nn.Sequential(
42            nn.Linear(layer1_0dim, class_num))
43
44    def forward(self, x):
45        x_i = self.input_layer(x)
46        x1 = self.layer1(x_i)
47        x2 = self.layer2(x1)
48        x3 = self.layer3(x2)
49        x4 = self.layer4(x3)
50
51        x3_ = self.decoder1(cat(x3, self.up1(x4)))
52        x2_ = self.decoder2(cat(x2, self.up2(x3_)))
53        x1_ = self.decoder3(cat(x1, self.up3(x2_)))
54        xi_ = self.decoder4(cat(x_i, self.up4(x1_)))
55        return self.output_layer(xi_)
```

Listing 4: Pseudo code of inflated ResNet for segmentation

```

1 Class LinearIO_3DRes_cls(nn.Module):
2     def __init__(self, res_block):
3         super().__init__()
4         # res_block means the residual block as same as the
4         conventional ResNet.
5         self.input_layer = nn.Sequential(
6             sparse_conv3d(input_dim, layer1_Idim, k=3, s=1),
7             sparse_bn(layer1_Idim))
8
9         self.layer1 = inflated_resnet_layer1(res_block, layer1_Idim,
10 layer1_0dim)
11         self.layer2 = inflated_resnet_layer2(res_block, layer2_Idim,
12 layer2_0dim)
13         self.layer3 = inflated_resnet_layer3(res_block, layer3_Idim,
14 layer3_0dim)
15         self.layer4 = inflated_resnet_layer4(res_block, layer4_Idim,
16 layer4_0dim)
17
18         self.output_layer = nn.Sequential(
19             global_average_pooling,
20             nn.Linear(layer4_0dim, class_num),
21             nn.bn(class_num))
22
23     def forward(self, x):
24         x = self.input_layer(x)
25         x = self.layer1(x)
26         x = self.layer2(x)
27         x = self.layer3(x)
28         x = self.layer4(x)
29         return self.output_layer(x)

```

Listing 5: Pseudo code of inflated ResNet with linear input and output for classification

```

1 Class LinearIO_3DRes_seg(nn.Module):
2     def __init__(self, res_block):
3         super().__init__()
4         # res_block means the residual block as same as the
4         conventional ResNet.
5         self.input_layer = nn.Sequential(
6             sparse_conv3d(input_dim, layer1_Idim, k=3, s=1),
7             sparse_bn(layer1_Idim))
8
9         self.layer1 = inflated_resnet_layer1(res_block, layer1_Idim,
10 layer1_0dim)
11         self.layer2 = inflated_resnet_layer2(res_block, layer2_Idim,
12 layer2_0dim)
13         self.layer3 = inflated_resnet_layer3(res_block, layer3_Idim,
14 layer3_0dim)
15         self.layer4 = inflated_resnet_layer4(res_block, layer4_Idim,
16 layer4_0dim)
17
18         self.up1 = sparse_deconv(layer4_0dim, layer4_0dim, k=2, s=2),
19 self.decode1 = self.Sequential(
20             sparse_conv3d(layer4_0dim+layer3_0dim, layer3_0dim, k=3, s
21 =1),
22             sparse_bn(layer1_Idim))
23
24         self.up2 = sparse_deconv(layer3_0dim, layer3_0dim, k=2, s=2)
25 self.decode2 = self.Sequential(
26             sparse_conv3d(layer3_0dim+layer2_0dim, layer2_0dim, k=3, s
27 =1),
28             sparse_bn(layer2_0dim))
29
30         self.up3 = sparse_deconv(layer2_0dim, layer2_0dim, k=2, s=2)
31 self.decode3 = self.Sequential(

```

```

26         sparse_conv3d(layer2_0dim+layer1_0dim, layer1_0dim, k=3, s
27         =1),
28         sparse_bn(layer1_0dim))
29
30     self.up4 = sparse_deconv(layer1_0dim, layer1_0dim, k=2, s=2)
31     self.decode4 = self.Sequential(
32         sparse_conv3d(layer1_0dim+layer1_0dim, layer1_0dim, k=3, s
33         =1),
34         sparse_bn(layer1_0dim))
35
36     self.output_layer = nn.Sequential(
37         nn.Linear(layer1_0dim, class_num))
38
39     def forward(self, x):
40         x_i = self.input_layer(x)
41         x1 = self.layer1(x_i)
42         x2 = self.layer2(x1)
43         x3 = self.layer3(x2)
44         x4 = self.layer4(x3)
45
46         x3_ = self.decoder1(cat(x3, self.up1(x4)))
47         x2_ = self.decoder2(cat(x2, self.up2(x3_)))
48         x1_ = self.decoder3(cat(x1, self.up3(x2_)))
49         xi_ = self.decoder4(cat(x_i, self.up4(x1_)))
50         return self.output_layer(xi_)

```

Listing 6: Pseudo code of inflated ResNet with linear input layer and the simplest decoder for segmentation

## 6.5 Stability analysis

We list the results of stability analysis in below tables. We run three trials to account for the randomness of experiments by changing the random seed. The results reported in our main body is one moderate value of the trials, and the results reported here is formed as mean  $\pm$  standard deviation. Note that we run 20, 15, and 10 trials for the experiment on data efficiency of 1% training data, 5% training data, and 10% training data, respectively (Table. 3 in the main paper).

Table 8: Stability analysis for Table. 1 in the main paper.

Layers to finetune	ModelNet(top 1 Acc%)	S3DIS(mIoU%)	SemanticKITTI(mIoU%)
I, O	79.32 $\pm$ 0.46	53.40 $\pm$ 0.25	55.74 $\pm$ 0.13
I, O, $\mu$ , $\sigma$	83.11 $\pm$ 0.23	54.82 $\pm$ 0.21	56.19 $\pm$ 0.11
I, O, $\mu$ , $\sigma$ , W, b	88.36 $\pm$ 0.17	55.26 $\pm$ 0.22	58.62 $\pm$ 0.14
whole network	88.87 $\pm$ 0.35	56.53 $\pm$ 0.21	65.33 $\pm$ 0.23
from scratch	88.65 $\pm$ 0.23	55.05 $\pm$ 0.17	64.66 $\pm$ 0.16
linear I, O	69.74 $\pm$ 0.45	48.83 $\pm$ 0.23	54.31 $\pm$ 0.14
linear network(w/o backbone)	8.91 $\pm$ 3.46	-	-
from scratch (linear I, O)	88.53 $\pm$ 0.36	54.79 $\pm$ 0.21	63.75 $\pm$ 0.29

Table 9: Stability analysis for Table. 2 in the main paper.

Layers to finetune	Tiny-ImageNet $\rightarrow$ ModelNet	Cityscapes $\rightarrow$ SemanticKITTI
	PointNet++ (Cls top 1 Acc%)	HRNetV2-W48 (Seg mIoU%)
I, O, $\mu$ , $\sigma$	82.14 $\pm$ 0.44	36.02 $\pm$ 0.11
whole network	90.64 $\pm$ 0.35	49.33 $\pm$ 0.11
from scratch	90.61 $\pm$ 0.33	44.09 $\pm$ 0.12

Table 10: Stability analysis for Table. 3 in the main paper.

Training data	1% data (20 trails)	5% data (15 trails)	10% data (10 trails)	100% data
w/ pretraining	$26.77 \pm 5.48$	$68.96 \pm 1.91$	$76.44 \pm 0.64$	$88.73 \pm 0.13$
w/o pretraining	$20.61 \pm 8.16$	$68.28 \pm 1.64$	$75.74 \pm 0.93$	$88.56 \pm 0.18$

Table 11: Stability analysis for Table. 4 in the main paper.

Layers to finetune	Tiny-ImageNet	ImageNet-1K	ImageNet-21K	FractalDB1K	FractalDB10K
	ModelNet (top 1 Acc.%)			ModelNet (top 1 Acc.%)	
I, O	$67.84 \pm 0.33$	$83.99 \pm 0.30$	$81.37 \pm 0.33$	$85.55 \pm 0.02$	$83.32 \pm 0.16$
I, O, $\mu$ , $\sigma$	$81.23 \pm 0.37$	$82.53 \pm 0.45$	$81.78 \pm 0.24$	$71.85 \pm 0.56$	$77.92 \pm 0.06$
I, O, $\mu$ , $\sigma$ , W, b	$88.86 \pm 0.48$	$88.92 \pm 0.22$	$89.46 \pm 0.20$	$88.36 \pm 0.30$	$88.57 \pm 0.18$
whole network	$88.84 \pm 0.14$	$88.73 \pm 0.13$	$89.21 \pm 0.04$	$88.48 \pm 0.07$	$88.55 \pm 0.14$
from scratch	$88.56 \pm 0.18$			$88.56 \pm 0.18$	

Table 12: Stability analysis for Table. 5 in the main paper.

Layers to finetune	ImageNet-1K	Cityscapes	ImageNet-1K	ADE20K
	SemanticKITTI (mIoU%)		S3DIS (mIoU%)	
I, O	$55.74 \pm 0.13$	$58.41 \pm 0.11$	$53.40 \pm 0.25$	$55.21 \pm 0.21$
I, O, $\mu$ , $\sigma$	$56.19 \pm 0.11$	$56.69 \pm 0.12$	$54.82 \pm 0.21$	$54.85 \pm 0.25$
I, O, $\mu$ , $\sigma$ , W, b	$58.62 \pm 0.14$	$59.47 \pm 0.17$	$55.26 \pm 0.22$	$55.28 \pm 0.25$
whole network	$65.33 \pm 0.23$	$65.51 \pm 0.22$	$56.53 \pm 0.21$	$56.22 \pm 0.24$
from scratch	$64.66 \pm 0.16$		$55.05 \pm 0.17$	

Table 13: Stability analysis for Table. 6 in the main paper.

Layers to finetune	ResNet-18	ResNet-50	ResNet-152
I, O	$79.32 \pm 0.46$	$83.99 \pm 0.30$	$69.42 \pm 0.08$
I, O, $\mu$ , $\sigma$	$83.11 \pm 0.23$	$82.53 \pm 0.45$	$81.16 \pm 0.38$
I, O, $\mu$ , $\sigma$ , W, b	$88.36 \pm 0.17$	$88.92 \pm 0.22$	$88.74 \pm 0.09$
whole network	$88.87 \pm 0.35$	$88.73 \pm 0.13$	$88.45 \pm 0.23$
from scratch	$88.65 \pm 0.23$	$88.56 \pm 0.18$	$88.75 \pm 0.02$

Table 14: Stability analysis for Table. 7 in the main paper.

To finetune	T1	T2	T3	ST	NST	ST(RI)	NST(RI)
I, O, $\mu$ , $\sigma$	$82.24 \pm 0.73$	$81.82 \pm 0.18$	$82.35 \pm 0.29$	$84.20 \pm 0.97$	$87.20 \pm 0.06$	$84.54 \pm 0.51$	$86.59 \pm 0.29$